Available online at www.sciencedirect.com

ScienceDirect

Materials and Design 28 (2007) 1142–1153

Materials & Design

www.elsevier.com/locate/matdes

Delamination of laminated fiber reinforced plastic composites under multiple cylindrical impact

Debabrata Chakraborty *

Department of Mechanical Engineering, Indian Institute of Technology Guwahati, Guwahati 781 039, Assam, India

Received 7 June 2005; accepted 24 January 2006
Available online 27 March 2006

Abstract

In the present paper a 3D finite element analysis has been performed for assessing delamination at the interfaces of graphite/epoxy laminated fiber reinforced plastic composites subjected to low velocity impact of multiple cylindrical impactors. Eight nodded layered solid elements have been used for the finite element analysis of fiber reinforced plastic laminates. Newmark-β method along with Hertzian contact law has been used for transient dynamic finite element analysis and an algorithm has been developed for determining the response of the laminated plate under the multiple impacts at different time. Appropriate delamination criterion has been used to assess the location and extent of delamination due to multiple impacts. A study has been carried out to observe the effects of important parameters on the impact response of the laminate and the delamination induced at the interfaces. It has been observed that the contact force magnitude as well as delamination at the interface are greatly influenced by the time interval between successive multiple impacts.

Keywords: Delamination; Graphite/epoxy; Impact; Multiple impacts; Finite element method

1. Introduction

Fiber reinforced plastic (FRP) laminated composites has been extensively used in aerospace and allied industries due to their inherent advantages like high strength to stiffness ratio. In spite of having these advantages, these materials are also susceptible to damages under transverse impacts and the nature of damage induced due to such impacts are entirely different than that in case of conventional metallic materials. In laminated FRP components, the damage mode usually consists of local permanent deformations, fiber breakage, delamination, matrix cracking, etc. Especially, in the case of impact low velocity impact, the resulting damages like, delamination occurs at specific interfaces of the laminate. These defects are sub surface in nature and cause considerable reduction in structural stiffness leading to growth of the damage and final fracture. Therefore, the impact response of laminated FRP composites has been an important area of research for long time. A large number of analytical as well as experimental works have already been reported in literature in this direction and some of the important works are discussed here.

Sun and Chattopadhyay [1] studied the contact force history of a simply supported laminate with initial stress subjected to impact loading by solving a non-linear integral equation. Sun and Chen [2] studied the impact response of initially stressed laminate using a 2D finite element analysis and reported the effects of impactor velocity, impactor mass and the initial stress on the impact response of the laminate. Wu and Chang [3] performed transient dynamic finite element analysis of laminated FRP plate subjected to impact of foreign objects and presented the stress and strain distribution through the laminate thickness during the impact. Choi and Chang [4,5] developed a model for damage initiation and the extent of damage as a function of material property, laminate configuration and impactor mass. Lee et al. [6] studied the impact response of hybrid-laminated composites under low velocity impact. Choi

* Tel.: +91 361 2582666; fax: +91 361 2690762.
E-mail address: chakra@iitg.ernet.in.

0261-3069/$ - see front matter © 2006 Elsevier Ltd. All rights reserved.
doi:10.1016/j.matdes.2006.01.029

and Hong [7] studied the frequency response of impact force history from modal analysis and compared the same with the natural frequency of the system where the mass of the impactor was lumped to the plate. Goo and Kim [8] studied the impact behavior of curved composite plates using penalty finite element method. Johnson et al. [9] developed a continuum damage mechanics model for studying the impact response and the delamination due to impact of a steel ball on a carbon/epoxy laminate. Guinard et al. [10] studied the localized damage due to transverse impact using a damage meso model for low velocity impact of laminated plates. Sung et al. [11] used acoustic emission along with wavelet transformation to detect matrix cracks and free edge delamination in graphite/epoxy laminates. Luo et al. [12] presented an approach for evaluation of impact damage initiation and propagation in composite plates using stress based delamination criterion.

McLaughlin and Santhanam [13] developed a 2D finite element model for simulating damage growth in cross ply symmetric laminates. Li et al. [14] developed a finite element based model for simulating low velocity impact induced damage in laminated composites and also used adaptive finite element analysis for increasing computational efficiency of the model. Duan and Ye [15] developed a 3D finite element model incorporating frictional contact for studying the delamination at the interfaces due to low velocity impact and showed excellent agreement with experimental results. Moura and Marques [16] performed numerical analysis and also conducted experiments to predict damages in carbon epoxy laminates subjected to low velocity impact. Zou et al. [17] developed a continuum damage model to study the delamination at the interfaces between constituent layers and compared the results with available experimental results. Tay et al. [18] developed an finite element code incorporating element failure algorithm to simulate dynamic crack propagation and impact damage in laminated composites subjected to low velocity impact. Krishnamurthy et al. [19] investigated the impact response of laminated composite cylindrical shell by classical as well as finite element method and studied the impact induced damage detection using finite element model. Shyr and Pan [20] investigated the damage characteristics and failure strengths of composite laminates at low velocity impact by performing experiments using a guided drop-weight test rig and observed that fiber breakage had occurred prior to the major damage. Aslan et al. [21] conducted experiments and also performed 3D finite element analysis to evaluate the delamination damage of E-Glass/epoxy laminated composites subjected to low velocity impact for evaluating delamination at various interfaces. Zhang and Taheri [22] performed experimental and numerical investigations for evaluating the damage in carbon epoxy laminated beam subjected to axial impact and observed that the density and length of delamination depend upon the stacking sequence. Mahanta et al. [23,24] performed adaptive finite element analysis for predicting contact force and delamination at the interfaces of laminated FRP components. Most of the works reported in the direction of impact response of laminated composites, are based on response under single impact only. Lam and Sathiyamoorthy [25] presented theoretical method to analyze the impact dynamics of a system, which consists of a laminated beam and multiple spherical masses by obtaining equation of motion using Lagrange equation.

Literature review reveals that many works have already been reported in the areas of assessment of delamination initiation under transverse impact in FRP composites. However, not many works are reported in the direction of study of delamination under multiple cylindrical impacts and the subsequent delamination due to multiple impacts on a laminated composite plate.

Therefore, the present work aims at performing a 3D transient dynamic finite element analysis of multiple impacts on FRP laminated plates for assessing the delamination at the interfaces. A code has been developed in C to study the contact force history, plate displacement and velocity history and impactor displacement and velocity history. The code developed has the capability to allow impactors of different masses striking with different velocities at different locations of the plate surface at different interval of time. Effect of various important parameters like impactor mass, impactor velocity and time interval between successive impacts on the impact response has been studied. Delaminations at interfaces between the constituent layers due to multiple impacts have been studied using the present code.

2. Problem definition

In the present work, response of a FRP composite plate subjected to multiple cylindrical impact (line-loading) impacts has been studied. Fig. 1 shows a laminated FRP composite plate of length L, width W and thickness h consisting of N laminae of different fiber orientation, clamped at its four edges and impacted by n number of cylindrical impactors of mass m_i and striking with an initial velocity of V_i $(i = 1, 2, 3 \ldots n)$. Appropriate contact laws have been assumed for the force–deformation relationship. The computation of contact force has been carried out for multiple impacts of different impactors striking the plate at different interval of time with different impactor velocities. Even though any location of the cylindrical impacts can be considered, in the present study, two impactors striking at symmetrical locations have been considered.

3. Finite element formulation

3.1. 8-Noded layered solid element

Three dimensional 8-noded isoparametric layered solid element was used for full 3D modeling of the laminated plate (Fig. 2). The shape function defining the geometry and displacement are

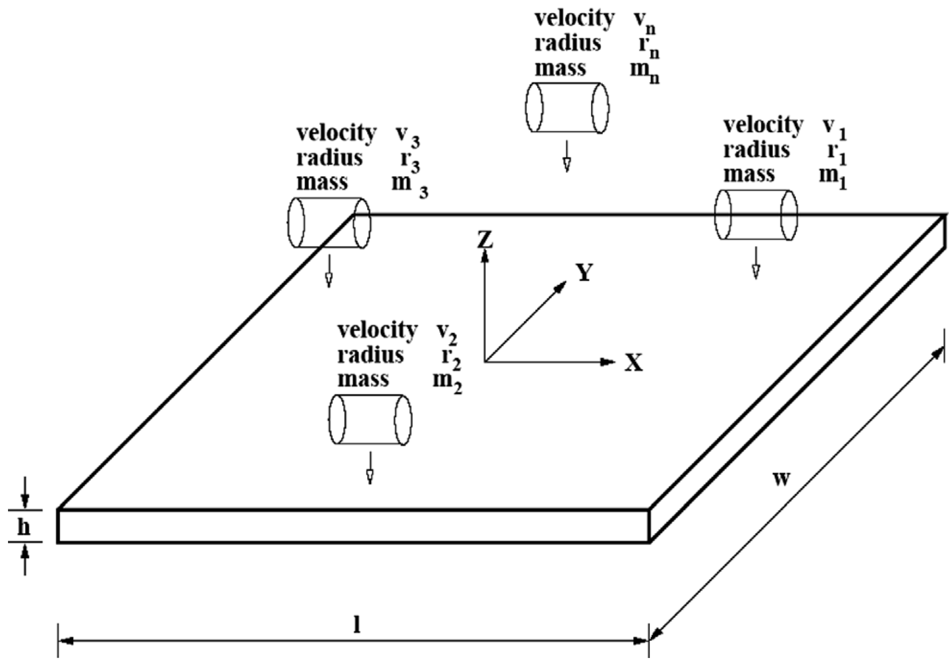

Fig. 1. Impact on a laminate by multiple cylindrical impactors.

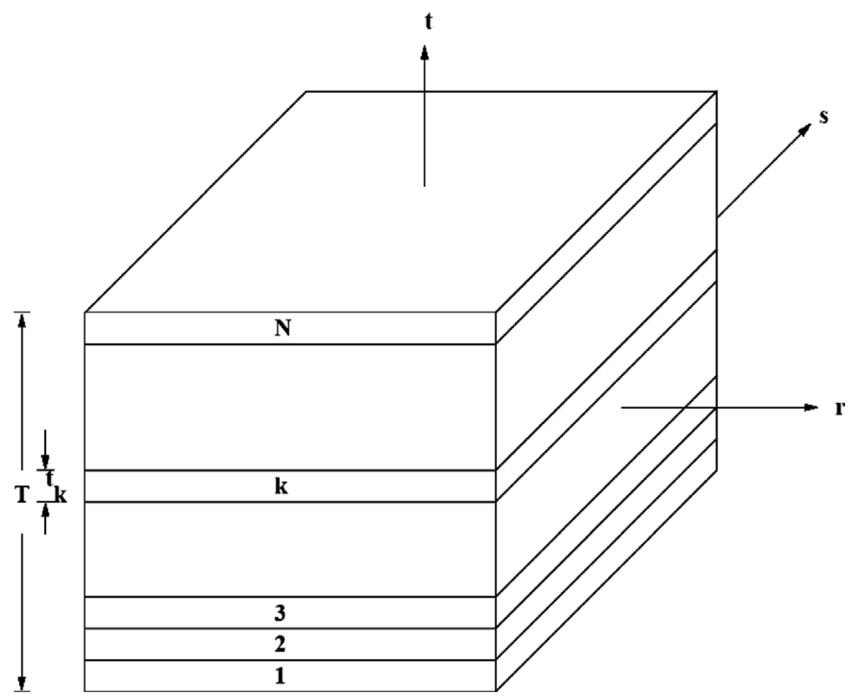

Fig. 2. Eight nodded 3D layered element.

$$N_i = \tfrac{1}{8}(1+rr_i)(1+ss_i)(1+tt_i) \quad i = 1,2,3,\ldots,8 \tag{1}$$

where r, s, t are natural coordinates and r_i, s_i, t_i are the values of natural coordinates for the ith node. In order to simulate the flexural response, extra shape functions are introduced to the general 8-noded solid element and they are

$$P_1 = (1-r^2) \quad P_2 = (1-s^2) \quad P_3 = (1-t^2) \tag{2}$$

The displacement variation within the element is given by

$$\{d\} = \begin{Bmatrix} u \\ v \\ w \end{Bmatrix} = \sum_{i=1}^{8} N_i \begin{Bmatrix} u_i \\ v_i \\ w \end{Bmatrix} + [P]\{\Psi\} \tag{3}$$

where

$$[P] = \begin{bmatrix} P_1 & P_2 & P_3 & 0 & 0 & 0 & 0 & 0 & 0 \\ 0 & 0 & 0 & P_1 & P_2 & P_3 & 0 & 0 & 0 \\ 0 & 0 & 0 & 0 & 0 & 0 & P_1 & P_2 & P_3 \end{bmatrix}$$

and

$$[\Psi]^{\mathrm{T}} = [\,\Psi_1 \quad \Psi_2 \quad \Psi_3 \quad \Psi_4 \quad \Psi_5 \quad \Psi_6 \quad \Psi_7 \quad \Psi_8 \quad \Psi_9\,]$$

The stiffness matrix is calculated as

$$[K] = \int_{-1}^{1}\int_{-1}^{1}\int_{-1}^{1}[B]^{\mathrm{T}}[C][B]|J|\,\mathrm{d}r\,\mathrm{d}s\,\mathrm{d}t \tag{4}$$

Let

$$G(r,s,t) = [B]^{\mathrm{T}}[C][B]|J| \tag{5}$$

then

$$[K] = \int_{-1}^{1}\int_{-1}^{1}\int_{-1}^{1}G(r,s,t)\,\mathrm{d}r\,\mathrm{d}s\,\mathrm{d}t \tag{6}$$

For an element having N layers in the thickness direction (Fig. 2),

$$T = \sum_{k=1}^{N} t_k \tag{7}$$

where T is the total thickness of the element and t_k is the thickness of the kth layer of the element. Taking a parameter $t\varepsilon[0,T]$ and changing the limits

$$[K] = \frac{2}{T}\int_{-1}^{1}\int_{-1}^{1}\sum_{k=1}^{N}\frac{t_k - t_{k-1}}{2}\int_{-1}^{1}F(r,s,t)\,\mathrm{d}r\,\mathrm{d}s\,\mathrm{d}t \tag{8}$$

where t is function of thickness over the layer.

$2\times2\times2$ Gauss quadrature scheme is applied to evaluate the above integration. The stiffness matrix thus evaluated by Eq. (8) is of size 33×33 and includes coefficients pertaining to the incompatible modes. Using static condensation technique these terms are eliminated and the condensed stiffness matrix becomes of the order of 24×24 pertaining to nodal degrees of freedom only. Element mass matrix is evaluated as

$$[M^{\mathrm{e}}] = \int_{V^m}[N]^{\mathrm{T}}\rho[N]\,\mathrm{d}v \tag{9}$$

3.2. Finite element contact impact modeling

Dynamic equation governing the impact problem (neglecting damping) at time $t+\Delta t$ is

$$[M]\{\ddot{d}\}^{t+\Delta t} + [K]\{d\}^{t+\Delta t} = \{F\}^{t+\Delta t} \tag{10}$$

where $[M]$ and $[K]$ are the mass and stiffness matrices and $\{F\},\{d\},\{\dot{d}\},\{\ddot{d}\}$ are force, displacement, velocity and acceleration vectors for plate, respectively, at time $t+\Delta t$. Using Newmark-β method, Eq. (10) can be reduced to

$$[\widehat{K}]\{d\}^{t+\Delta t} = \{\widehat{F}\}^{t+\Delta t} \tag{11}$$

where $[\widehat{K}]$ is the effective stiffness matrix and $[\widehat{F}]$ is the effective force vector and are defined as

$$[\widehat{K}] = \frac{1}{\Phi\Delta t^2}[M] + [K] \tag{12}$$

$$\{\widehat{F}\} = \{H\}^t + \{F\}^{t+\Delta t} \tag{13}$$

$$\{H\}^t = [M]\left(\frac{1}{\Phi\Delta t^2}\{d\}^t + \frac{1}{\Phi\Delta t}\{\dot{d}\} + \left(\frac{1}{2\Phi} - 1\right)\{\ddot{d}\}\right) \tag{14}$$

where ϕ and δ are the Newmark constants.

In Eq. (11), displacement, velocity and acceleration at time t are known at each point inside the plate and the unknown quantities in this equation are vector $\{d\}^{t+\Delta t}$ and the force vector $\{F\}^{t+\Delta t}$. In the absence of pre-load, Eq. (11) becomes

$$[\widehat{K}]\{d\}^{t+\Delta t} = \{H\}^t + \{P\}^{t+\Delta t} \tag{15}$$

where $\{P\}$ is the contact force.

The displacement vector $\{d\}$ is expressed as the sum of the displacements due to the force $\{H\}$ and the contact force $\{P\}$ as

$$\{d\}^{t+\Delta t} = \{d\}_H^{t+\Delta t} + \{d\}_P^{t+\Delta t} \tag{16}$$

Eqs. (15) and (16) give

$$[\widehat{K}]\{d\}_H^{t+\Delta t} = \{H\}^t \tag{17}$$

and

$$[\widehat{K}]\{d\}_P^{t+\Delta t} = \{P\}^{t+\Delta t} \tag{18}$$

Writing $\{P\}^{t+\Delta t} = f^{t+\Delta t}\{U\}$, where $f^{t+\Delta t}$ is the magnitude of contact force at time $t+\Delta t$. Eq. (18) yields

$$[\widehat{K}]\{d\}_P^{t+\Delta t} = f^{t+\Delta t}\{U\} \tag{19}$$

and for a unit contact force ($f^{t+\Delta t} = 1$)

$$[\widehat{K}]\{d\}_U^{t+\Delta t} = \{U\} \tag{20}$$

where $\{d\}_U^{t+\Delta t}$ is the displacement caused by the unit contact force and

$$\{d\}_P^{t+\Delta t} = f^{t+\Delta t}\{d\}_U^{t+\Delta t} \tag{21}$$

Eqs. (17) and (21) give

$$\{d\}^{t+\Delta t} = \{d\}_H^{t+\Delta t} + f^{t+\Delta t}\{d\}_U^{t+\Delta t} \tag{22}$$

3.2.1. Contact of a cylinder with a plate

When a plate is impacted by a mass, the magnitude of contact force, which results because of the impact, is not known a priori. This contact force needs to be calculated before the plate motion is analysed. The evaluation of contact force depends on a contact law, which relates the contact force with the indentation.

A Hertizian distribution of pressure is assumed to act on plane, which is uniform along the length of barreled cylinder. In order to reduce stress concentration at ends, the axial profile of the cylinder should be slightly barreled. The contact force is given by [26]

$$f = \frac{\pi l E^*\delta}{1.886 + \ln(l/a)} \tag{23}$$

where δ is displacement at the center of contact. $2l$ is the length of the cylinder in contact and a is given by

$$a = \sqrt{\frac{4fr}{\pi E^*}} \quad \text{and} \quad \frac{1}{E^*} = \frac{1-v_i^2}{E_i} + \frac{1-v^2}{E} \tag{24}$$

where, r is radius of the cylinder, E_i and E are Young's modulii of impactor and target normal to the fiber direction in the uppermost composite layer, respectively. v_i and v are Poisson's ratios of impactor and target, respectively. Eq. (23) is considered as the relationship between indentation and contact force both for loading and unloading.

At time $t+\Delta t$ this depth is

$$\delta^{t+\Delta t} = \delta_S^{t+\Delta t} - \delta_C^{t+\Delta t} \tag{25}$$

Here $\delta_S^{t+\Delta t}$ is the position of the center point of the impactor and $\delta_C^{t+\Delta t}$ is the displacement of the center of the mid surface of the plate in the direction of impact. At time $t+\Delta t$, magnitude of $\delta_S^{t+\Delta t}$ can be determined by Newton's second law as

$$\delta_S^{t+\Delta t} = \int_0^{t+\Delta t} v\,dt + \int_0^{t+\Delta t}\int_0^{t+\Delta t} \frac{f}{m}\,dt\,dt \tag{26}$$

Using Eq. (25)

$$\delta_C^{t+\Delta t} = \delta_{CH}^{t+\Delta t} + f^{t+\Delta t}\delta_{CU}^{t+\Delta t} \tag{27}$$

Combining Eqs. (25)–(30) the following expressions for the contact force are obtained

$$f^{t+\Delta t} = \frac{\pi l E^*}{1.886 + \ln(l/a)}\left(\int_0^{t+\Delta t} v\,dt + \int_0^{t+\Delta t}\int_0^{t+\Delta t}\frac{f}{m}\,dt\,dt - \delta_{CH}^{t+\Delta t} - f^{t+\Delta t}\delta_{CU}^{t+\Delta t}\right) \tag{28}$$

Contact force at $t+\Delta t$, i.e. $f^{t+\Delta t}$ was calculated using Eq. (28) (during loading or during unloading) by Newton Raphson method. From the known value of contact force $f^{t+\Delta t}$, displacement vector $\{d\}^{t+\Delta t}$ is calculated using Eq. (22). Once the value of $f^{t+\Delta t}$ is known, plate velocity, acceleration and then the stresses and strains at time $t+\Delta t$ was calculated. This procedure has been repeated for each time step to get the displacement, stress and strain.

3.2.2. Stress based criterion for delamination

In order to assess delamination initiation at the interface of the laminate, the criterion proposed by Choi et al. [4,5] for impact induced delamination has been used in the present work. The criterion is

$$D_a\left[\left(\frac{\bar{\sigma}_{yz}^n}{S_i^n}\right)^2 + \left(\frac{\bar{\sigma}_{xz}^{n+1}}{S_i^{n+1}}\right)^2 + \left(\frac{\bar{\sigma}_{yy}^{n+1}}{Y^{n+1}}\right)^2\right] = e_D^2 \tag{29}$$

where

$$\begin{aligned} &e_D \geqslant 1 \text{ failure} \\ &e_D < 1 \text{ no failure} \\ &Y^{n+1} = Y_t^{n+1} \quad \text{if } \bar{\sigma}_{yy} \geqslant 0 \\ &Y^{n+1} = Y_c^{n+1} \quad \text{if } \bar{\sigma}_{yy} < 0 \end{aligned} \tag{30}$$

and D_a is an empirical constant determined from experiment, which has been taken as 1.8 as suggested by Choi et al. [4]. $\bar{\sigma}_{xz}$, $\bar{\sigma}_{yz}$ and $\bar{\sigma}_{yy}$ are average stresses in the interface between nth and $n+1$th ply, respectively, and are expressed as

$$[\bar{\sigma}_{xz,yz,yy}^{n+1}] = \frac{1}{h_{n+1}}\int_{t_{n-1}}^{t_n}[\sigma_{xz,yz,yy}]\,dt \tag{31}$$

3.2.3. Multiple impact algorithm

Based on the formulation described above, analysis of multiple cylindrical impacts on the FRP plate has been implemented as follows:

Define time step Δt

For each impact i:

Solve for $\{d_p\}_i$ from $\left[\widehat{K}\right]\{d_i\}_p^{t+\Delta t} = \{U_i\}$

$\{d_p\}$ is displacement due to unit load at contact point in impact direction

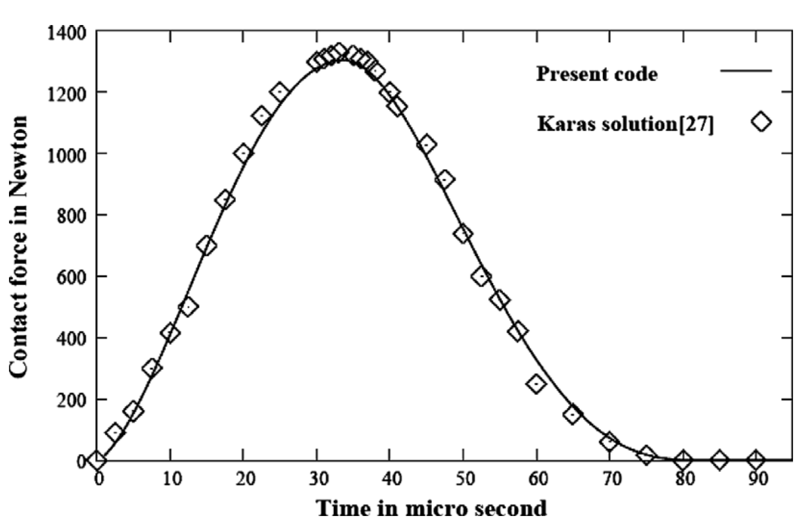

Fig. 3a. Contact force history for a steel ball impacting on an isotropic plate.

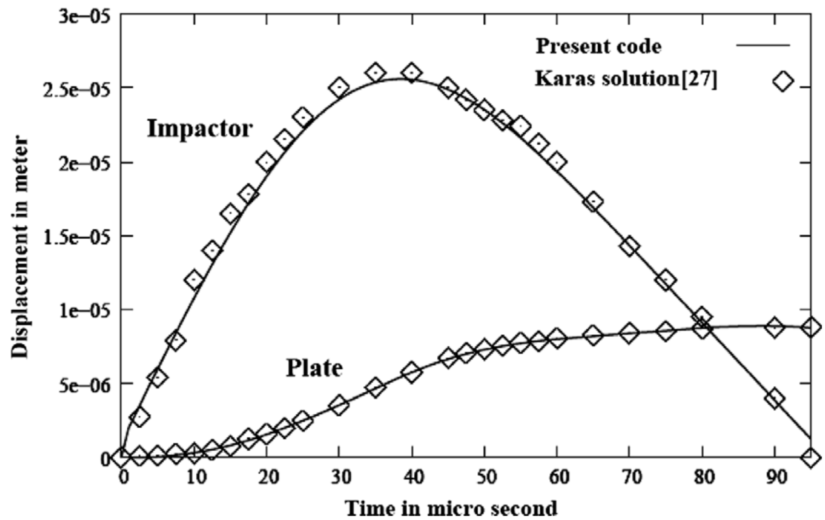

Fig. 3b. Plate and impactor displacement for a steel ball impacting on a steel plate.

For each time step:

1. Calculate $\{H\}^t = [M]\{a_0 d^t + a_2 \dot{d}^t + a_3 \ddot{d}^t\}$.
2. Solve for d_H from $[\widehat{K}]\{d\}_H^{t+\Delta t} = \{H\}^t$.
3. *For each impact i:*
   If (impact time < time at time step)
   Calculate contact force $f_i^{t+\Delta t}$ using Eq. (28)
   Else
   Contact force $f_i^{t+\Delta t} = 0$
4. Calculate displacement using

$$\{d\}^{t+\Delta t} = \{d\}_H^{t+\Delta t} + \sum_{i=1}^{N} f_i^{t+\Delta t}\{d_p\}_i \quad \text{where } N \text{ number of impacts}$$

5. Calculate acceleration and velocity using

$$\{\ddot{d}\}^{t+\Delta t} = a_0\left(\{d\}^{t+\Delta t} - \{d\}^t\right) - a_2\{\dot{d}\}^t - a_3\{\ddot{d}\}^t$$

$$\{\dot{d}\}^{t+\Delta t} = \{d\}^t + a_6\{\ddot{d}\}^t + a_7\{\ddot{d}\}^{t+\Delta t}$$

6. Calculate displacement due to incompatible modes.
7. Calculate strains and stresses.
8. Apply failure criteria to assess delamination.

Go to next time step

Table 1
Mechanical properties of unidirectional graphite/epoxy lamina

Ply thickness, h	1.5875×10^{-4} m
Density, ρ	1535.68 Kg/m^3
Longitudinal Young's modulus, E_{xx}	1.454×10^{11} N/m^2
Transverse, Young's modulus, E_{yy}	9.99×10^9 N/m^2
Shear modulus in x–y direction, G_{xy}	5.68845×10^9 N/m^2
Poisson's ratio in x–y direction, v_{xy}	0.3
Poisson's ratio in y–z direction, v_{yz}	0.3
Longitudinal tensile strength, Y_{LT}	1.778×10^9 N/m^2
Longitudinal compressive strength, Y_{LC}	1.731×10^9 N/m^2
Transverse tensile strength, Y_{ten}	5.520×10^7 N/m^2
Transverse compressive strength, Y_C	2.940×10^8 N/m^2
Interlaminar shear strength, S_i	1.012×10^8 N/m^2

4. Results and discussion

4.1. Computer code and validation

Based on the analytical model described above, a computer code has been developed in C language for

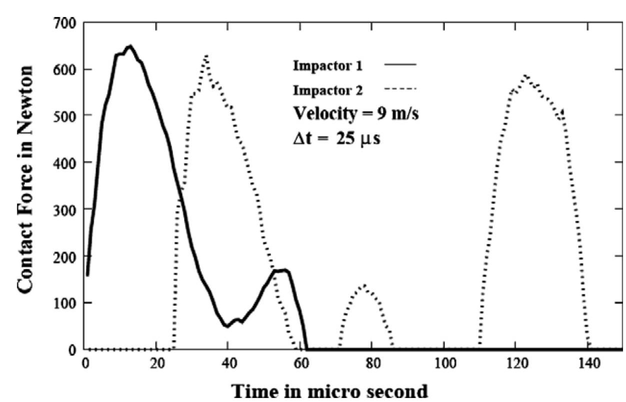

Fig. 4a. Contact force history two successive impacts on $[0/-45/45/90]_{2S}$ graphite/epoxy plate.

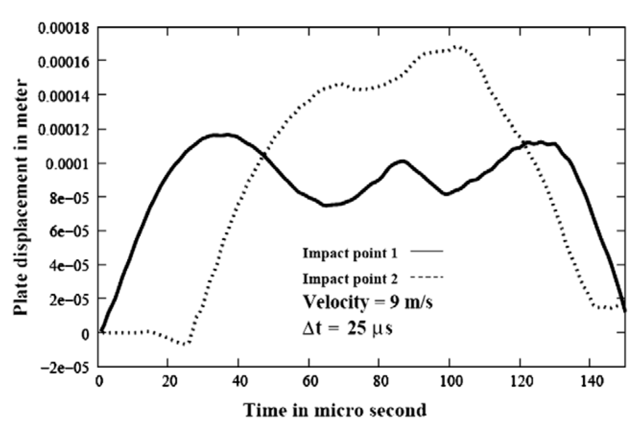

Fig. 4b. Plate displacement history for two successive impacts on $[0/-45/45/90]_{2S}$ graphite/epoxy plate.

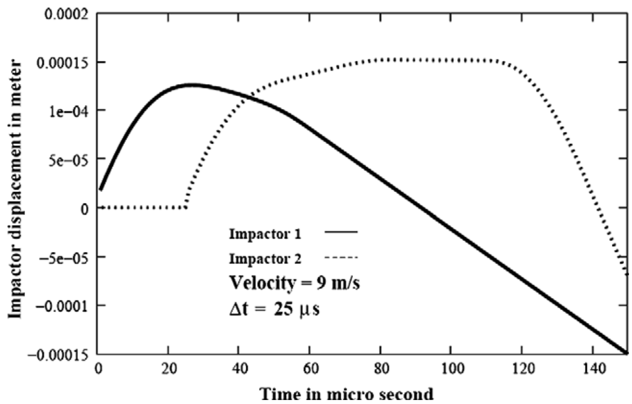

Fig. 4c. Impactor displacement history for two successive impacts on $[0/-45/45/90]_{2S}$ graphite/epoxy plate.

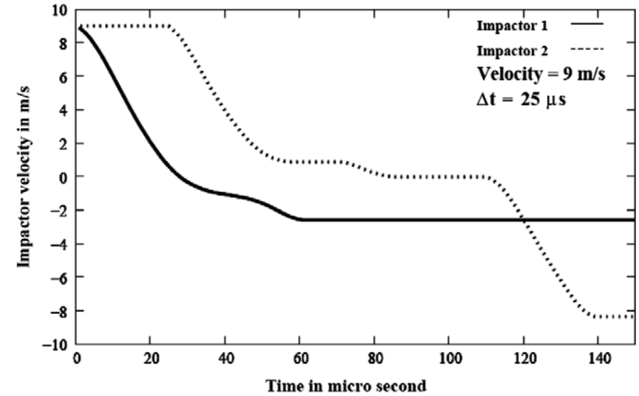

Fig. 4e. Impactor velocity history for two successive impacts on $[0/-45/45/90]_{2S}$ graphite/epoxy plate.

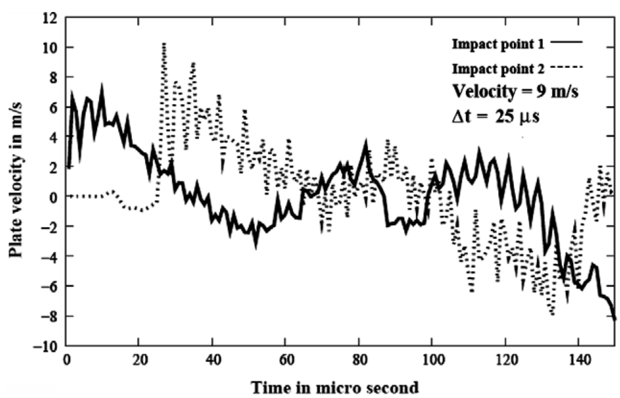

Fig. 4d. Plate velocity history for two successive impacts on $[0/-45/45/90]_{2S}$ graphite/epoxy plate.

finite element contact impact analysis of a FRP laminate. The FE code has been verified by comparing the results obtained from the present code for a steel ball impacting on a steel plate with the analytical solution of Karas [27] and excellent agreements have been obtained. Figs. 3a and 3b show the comparison of contact force history and the plate and impactor displacement history results obtained from the present code and the solution of Karas.

4.2. Two cylindrical impactors striking at different time

A laminated plate made of T300/934 graphite/epoxy with ply orientation of $[0/-45/45/90]_{2S}$ is clamped along all the four edges and is impacted by two cylindrical impactors which strike at equally offset locations from the ends and are symmetrically located. Table 1 shows the mechanical properties of T300/934 graphite epoxy. Plate and impactor geometry and other configurations are as follows:

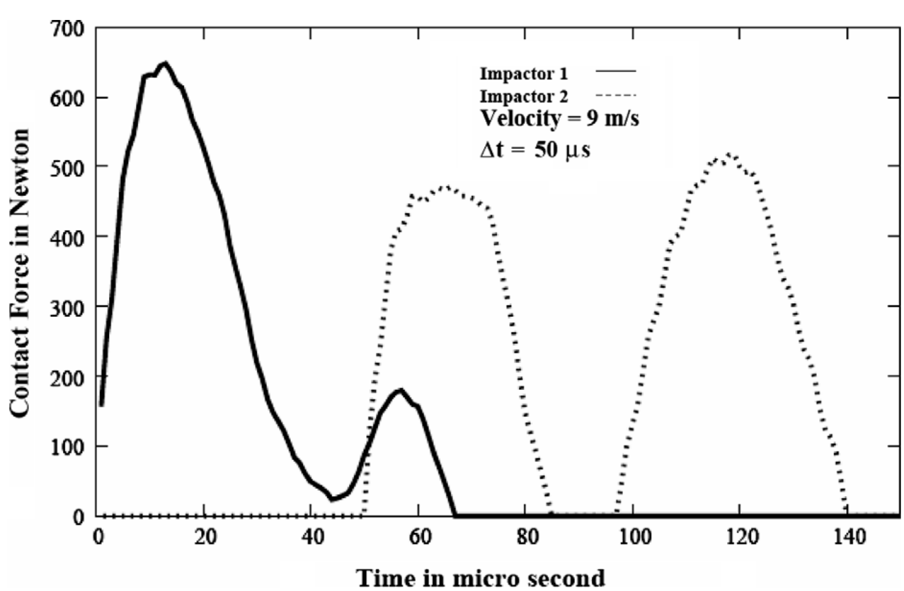

Fig. 5a. Contact force history for two successive impacts on $[0/-45/45/90]_{2S}$ graphite/epoxy plate.

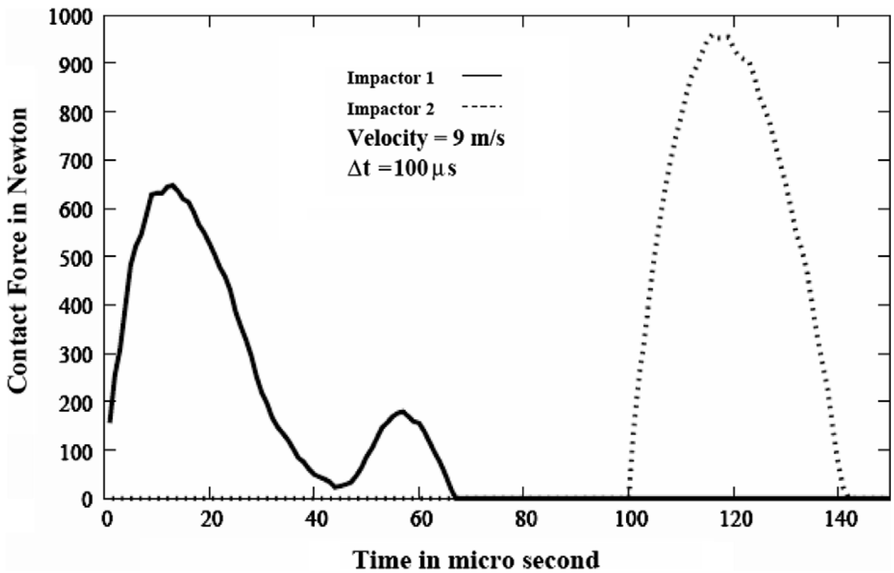

Fig. 5b. Contact force history for two successive impacts on $[0/-45/45/90]_{2S}$ graphite/epoxy plate.

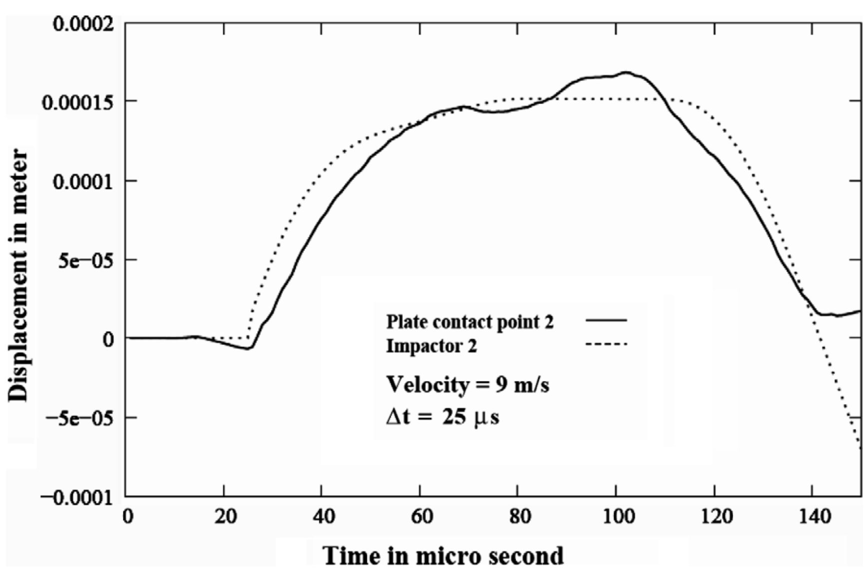

Fig. 6a. Displacements of second impactor and the corresponding contact point of the $[0/-45/45/90]_{2S}$ graphite/epoxy plate.

Dimensions of plate	0.0762 m × 0.0762 m × 0.00254 m
Diameter of cylindrical impactors	0.0050 m
Length of the cylinder	0.020 m
Two locations of contact	(0.01905, 0.0381,0.00254)and (0.57150,0.0381,0.00254)
Time step	1 μs
FEM mesh	20 × 20 × 2

In this case, the two impactors strike the plate at a time interval for Δt seconds between them i.e. the second impactor strikes the plate after a definite time after the first impact. In the present work, three cases of time interval has been considered viz. for $\Delta t = 25$, 50 and 100 μs to study the effect of time interval between successive impacts on the plate response. The velocity of the impactors has been taken as 9 m/s. Fig. 4a shows contact force history when second impactor hits the plate of 25 μs after the first impact. In this figure as well as in all the subsequent figures results are plotted up to 150 μs, even though the code has been run for 300 μs. Since in all the cases studied here, contact has been observed to completely lost after 150 μs, for clarity of figures, all the histories (force, displacement, velocity) have been plot up to 150 μs. It has been observed from the figure that the first impactor comes in contact only once and the second impactor comes in contact three times before the contact is completely lost. Figs. 4b and 4c

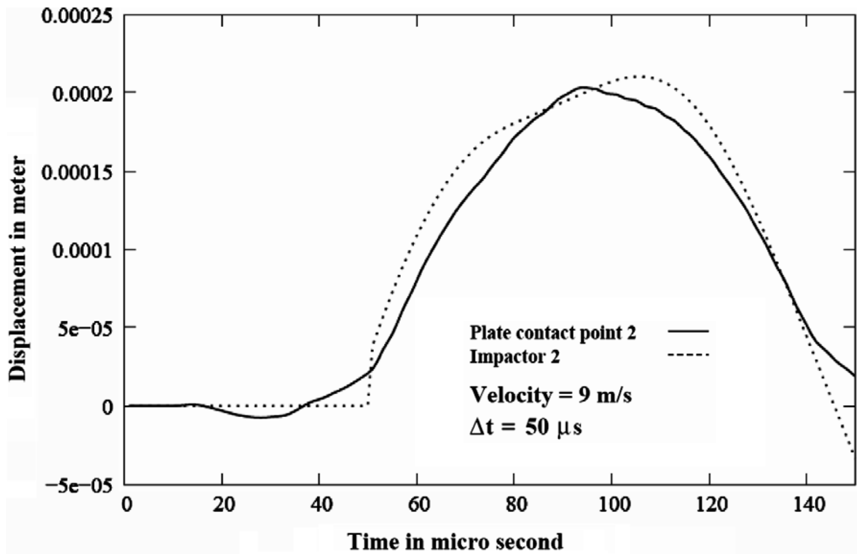

Fig. 6b. Displacements of second impactor and the corresponding contact point of the $[0/-45/45/90]_{2S}$ graphite/epoxy plate.

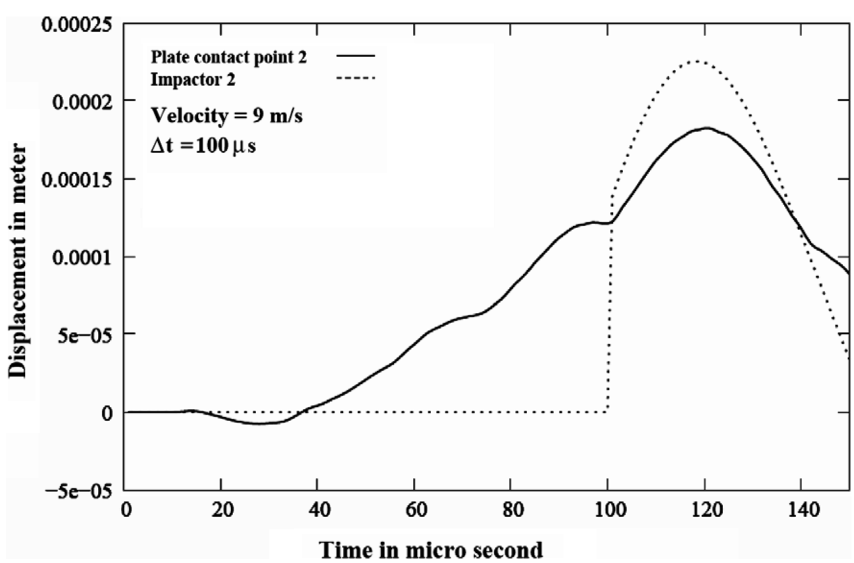

Fig. 6c. Displacements of second impactor and the corresponding contact point of the $[0/-45/45/90]_{2S}$ graphite/epoxy plate.

show the plate and impactor displacement histories and it could be observed that the plate displacement at the second contact point is more compared to that of first contact point. Figs. 4d and 4e show the velocity histories of the plate and the impactor, respectively. As expected the plate velocity is more at the second contact point compared to that at the first contact point. Also, due to reloading of the second impactor the rebounding velocity of the second impactor is more compared to that of the first impactor. Figs. 5a and 5b show the contact force histories for successive impacts for time intervals of 50 and 100 μs, respectively. Comparing the contact force histories of the three cases of increasing time intervals (Figs. 4a, 5a and 5b), it could be observed that as the time interval between two successive impacts increases, the magnitude of contact force for the second impactor changes. In the present case, the magnitude of the contact force due to the second impactor is less when $\Delta t = 50$ μs compared to that in case of $\Delta t = 25$ μs. However, the contact force magnitude is much more in the case of $\Delta t = 100$ μs. This is due to the fact that the second contact point of the plate and the impactor were moving opposite to each other at the time of contact in the case of $\Delta t = 25$ μs and $\Delta t = 100$ μs leading to higher magnitude of contact force at the impact point. However in the case of $\Delta t = 50$ μs, both the contact point and the impactor were moving in the same direction leading to comparatively lower magnitude of contact force. This could be clearly observed from Figs. 6a, 6b and 6c showing the displacement of the second impactor and the corresponding contact point of the plate. Fig. 7 shows the delaminations at the three interfaces viz. 1, 2 and 3 for two successive impacts for three cases of time interval between the successive impacts (for $\Delta t = 25$ μs, $\Delta t = 50$ μs and $\Delta t = 100$ μs). It could be observed that the direction of delamination is dependent on the fiber orientation of the adjacent ply, which is an already established result [5]. This is more visible in the case of two successive impacts with $\Delta t = 100$ μs. In all the three cases studied here, both the impactors strike with a velocity of 9 m/s. It has been observed that the shape of the delamination is not symmetric as expected due to impacts at different time. It could also be observed from the figures that for less time interval between two successive impacts, two delaminations starting from the two impact locations coalesce into one big delamination. However, as the time interval between the successive impacts increases, the delaminations remain as two distinct delaminations and do not coalesce into one. This is due to the fact that, in the case of larger time interval between the two successive impacts, contact at the first impact site is lost before the second contact begins which is clear from the contact force histories for different Δt values. Therefore in the case of large $\Delta t = 100$ μs, the chances of further delaminations near the first contact point is less. Hence the two delaminations do not coalesce in to one big delamination. This, however, will also depend upon the distance between the two impact points. It has been observed that the extent of delamination is more when the interval between successive impacts is less. Fig. 8 shows how the delamination at interface 2 grows with time. Before the second impactor strikes, delamination is limited to the zone surrounding the fist impact point only. As the second impact takes place,

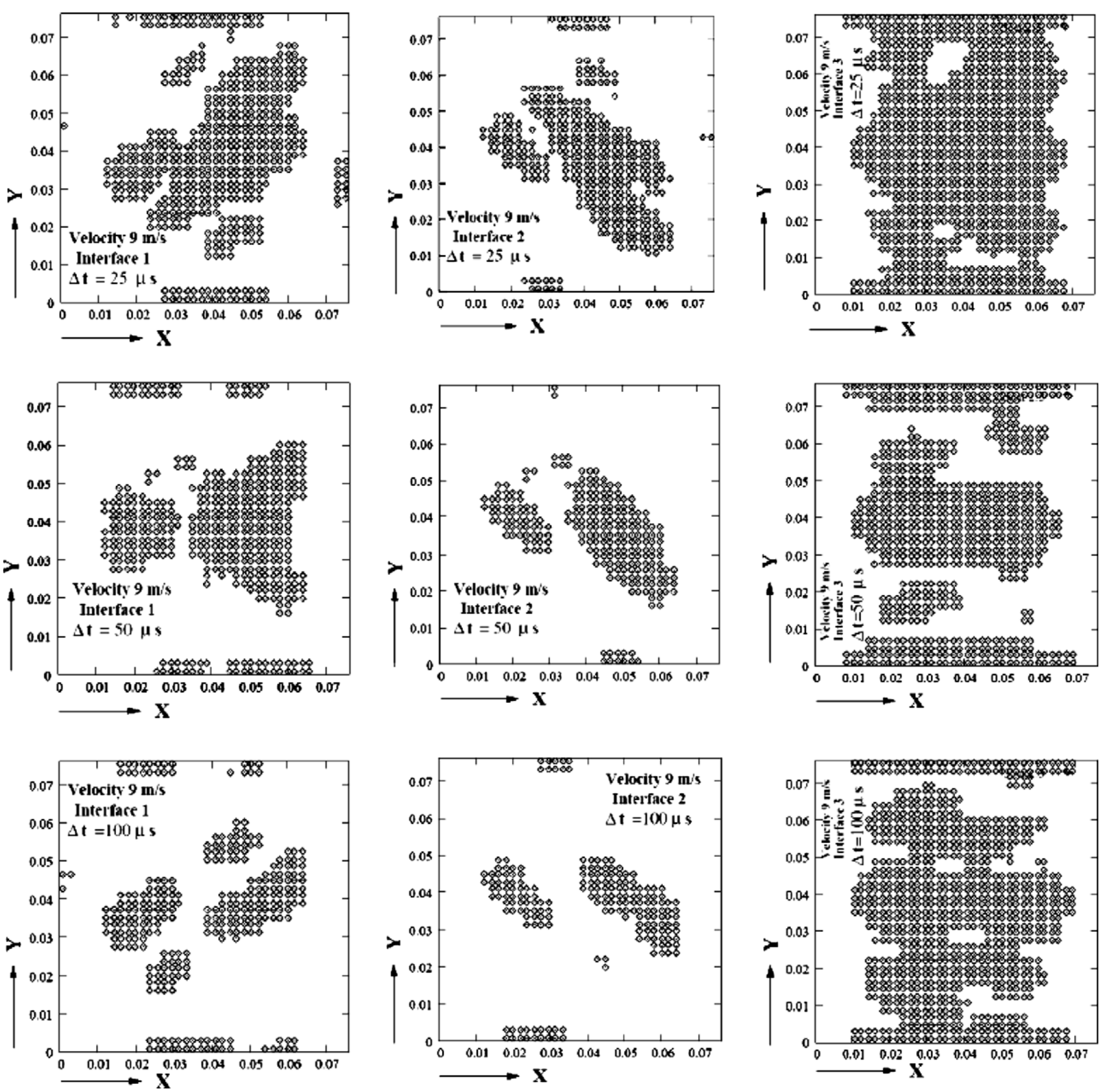

Fig. 7. Delamination at the interfaces 1, 2 and 3 due to two successive impacts on $[0/-45/45/90]_{2S}$ graphite/epoxy plate at different time interval between two impacts with a velocity of 9 m/s.

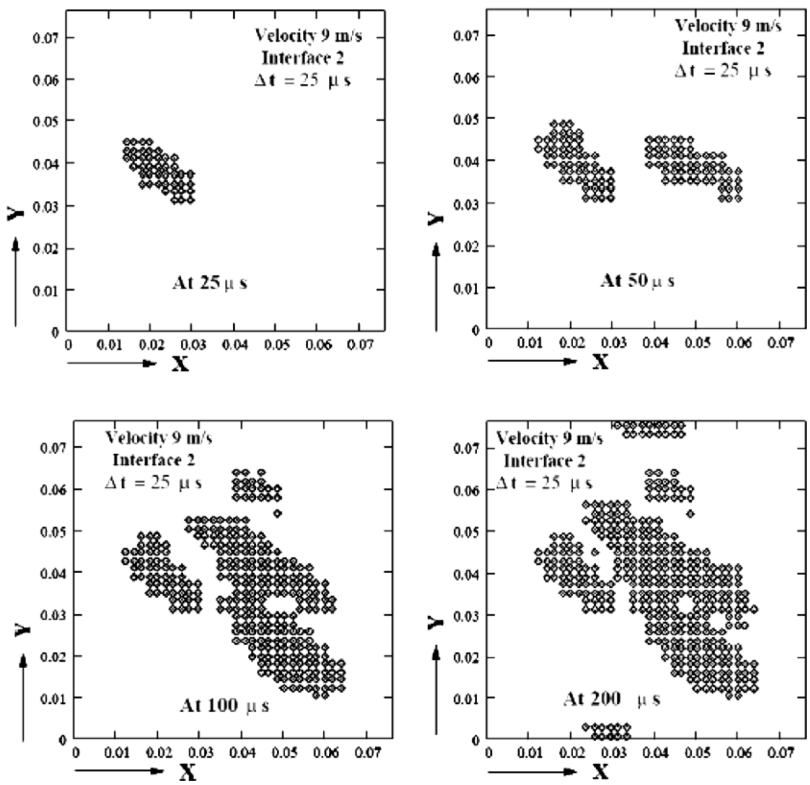

Fig. 8. Delamination at interface 2 due to two successive impacts on $[0/-45/45/90]_{2S}$ graphite/epoxy plate at 25 μs time interval between two impacts with a velocity of 9 m/s.

delamination starts growing at that location also and at the end, two delaminations coalesces to form one single delamination. However whether delamination will grow into one single delamination or remain two distinct delamination depends upon the time interval between the two impacts as well as the distance between the two impact points.

5. Conclusions

A 3D finite element code for analysis of multiple cylindrical impacts on FRP laminated plate has been developed. The code is quite general in terms of number of impactors, time of impacts and location of impacts. Contact force histories, plate and impactor displacement, plate and impactor velocities have been studied for two successive cylindrical impacts and the subsequent delaminations at the interfaces due to such impacts have been assessed. Presnt work lead to the following important conclusions:

1. In case of multiple impacts, magnitude of contact force at various impact points depend upon the time interval between successive impacts in addition to mass and velocity of the imapactors. Depending upon the relative velocities of the plate and the impactor at the time of contact magnitude of contact force will be different.
2. In case of multiple impacts, delaminations start from two distinct zones surrounding the impact points. However whether two delaminations will coalesce into one single delamination or remain two distinct delaminations depend upon the time interval of successive impacts in addition to the impactor velocity and the distance between the two impact points.
3. Delaminations at an interface near the impact points remain distinct for increasing time interval between the successive impacts. For quicker successive impacts, they coalesce into one big delamination.

References

[1] Sun CT, Chattopadhyay S. Dynamic response of anisotropic laminated plates under initial stress to impact of a mass. J Appl Mech 1975;42:693–8.
[2] Sun CT, Chen JK. On the impact of initially stressed composite laminates. J Compos Mater 1985;19:490–504.
[3] Wu Hsi-Yung T, Chang FK. Transient dynamic analysis of laminated composite plate subjected to transverse impact. Comput Struct 1989;31(3):453–66.
[4] Choi HY, Wu Hsi-Yung T, Chang FK. A new approach towards understanding damage mechanism and mechanics of laminated composites due to low velocity impact: Part II – analysis. J Compos Mater 1991;25:1012–38.
[5] Choi HY, Chang FK. A model for predicting damage in graphite/epoxy laminated composite resulting from low-velocity point impact. J Compos Mater 1992;26(14):2134–69.
[6] Lee YS, Kang KH, Park O. Response of hybrid laminated composite plates under low-velocity impact. Comput Struct 1994;65(5):965–74.
[7] Choi IH, Hong CS. New approach for simple prediction of impact force history on composite laminates. AIAA J 1994;32(10):2067–72.

[8] Goo NS, Kim SJ. Dynamic contact analysis of laminated composite plates under low-velocity impact. AIAA J 1997;35(9):1518–21.
[9] Johnson AF, Pickett AK, Rozycki P. Computational methods for predicting impact damage in composite structures. Compos Sci Technol 2001;61:2183–92.
[10] Guinard S, Allix O, Gue' dra-Degeorges D, Vinet A. A 3D damage analysis of low-velocity impacts on laminated composites. Compos Sci Technol 2002;62:585–9.
[11] Sung D, Kim CG, Hong CS. Monitoring of impact damages in composite laminates using wavelet transform. Composites Part B 2002;33:35–43.
[12] Luo RK, Green ER, Morrison CJ. An approach to evaluate impact damage initiation and propagation in composite plates. Composites Part B 2002;32:513–20.
[13] McLaughlin PVD, Santhanam S. Simulating damage growth in a [90/0]s composite laminate using quasi-two-dimensional finite element methods. Compos Struct 2002;58:227–36.
[14] Li CF, Hu N, Yin YJ, Sekine H, Fukunaga H. Low-velocity impact-induced damage of continuous fiber-reinforced composite laminates. Part I. An FEM numerical model. Composites Part A 2002;33:1055–62.
[15] Duan SH, Ye TQ. Three dimensional frictional dynamic contact analysis for predicting low velocity impact damage in composites. Adv Eng Software 2002;33:9–15.
[16] de Moura MFSF, Marques AT. Prediction of low velocity impact damage in carbon epoxy laminates. Composites Part A 2002;33:361–8.
[17] Zou Z, Reid SR, Li S. A continuum damage model for delaminations in laminated composites. J Mech Phys Solid 2003;51:333–56.
[18] Tay TE, Tan VBC, Deng M. Element-failure concepts for dynamic fracture and delamination in low-velocity impact of composites. Int J Solid Struct 2003;40:555–71.
[19] Krishnamurthy KS, Mahajan P, Mittal RK. Impact response and damage in laminated composite cylindrical shells. Compos Struct 2003;59:15–36.
[20] Shyr TW, Pan YH. Impact resistance and damage characteristics of composite laminates. Compos Struct 2003;62:193–203.
[21] Aslan Z, Karakuzu R, Okutan B. The response of laminated composite plates under low-velocity impact loading. Compos Struct 2003;59:119–27.
[22] Zhang Z, Taheri F. Dynamic damage initiation of composite beams subjected to axial impact. Compos Sci Technol 2004;64(5):719–28.
[23] Mahanta BB, Reddy P, Dutta A, Chakraborty D. Reliable computation of contact force in FRP composite laminates under transverse impact. Shock Vib 2004;11:129–42.
[24] Mahanta BB, Chakraborty D, Dutta A. Accurate prediction of delamination in FRP composite laminates resulting from transverse impact. Compos Sci Technol 2004;64:2341–51.
[25] Lam KY, Sathiyamoorthy TS. Response of composite beams under low-velocity impact of multiple masses. Compos Struct 1999;44:205–20.
[26] Johnson KL. Contact mechanics. Cambridge University Press; 1996.
[27] Karas K. Platten unter seitchem stoss. Ingenieur Archiv 1939;10:237–50.